American Mineralogist, Volume 73, pages 172–180, 1988

Optical absorption spectroscopy of natural and irradiated pink tourmaline

Marly Bueno de Camargo, Sadao Isotani
Instituto de Física, Universidade de São Paulo, C.P. 20516, 01498 São Paulo, SP, Brazil

Abstract

We have studied the Brazilian natural pink tourmaline through polarized optical absorption measurements. The effects of increasing doses of γ-rays from ^{60}Co on the spectra were determined (maximum of 20 MGy). The following optical absorption bands were observed: 8500 and 14 800 cm^{-1} assigned to *d-d* transitions of Fe^{2+} in b and c sites, respectively; 19 500 and 25 500 cm^{-1} assigned to $^5E \rightarrow {}^5A_1$ and $^5B_2 \rightarrow {}^5A_1$ *d-d* transitions of Mn^{3+}, respectively.

Introduction

Tourmaline is a silicate mineral whose chemical composition, $NaX_3Al_6B_3Si_6O_{27}(OH,F)_4$, is extremely complex. The X sites can be occupied by several ions, which explains the great number of varieties of tourmaline found in nature. There is a continuous series between schorl (X = Fe,Mn) and elabaite (X = Li,Al), and another one between dravite (X = Mg) and schorl. There is a compositional gap between dravite and elbaite that is reflected in the variation of the lattice parameters *a* and *c* obtained by Barton (1969). Tourmaline has a hardness of 7 on the Mohs' scale. Its space group (Townsend, 1970; Webster, 1980; Wilkins et al., 1969) is $R3m$. In general, the crystals are prismatic with a trigonal prism and a subordinant second-order hexagonal prism. Its density ranges from 3.02 to 3.26 g/cm^3, and the refractive indexes range between 1.62 and 1.64. The unit-cell dimensions vary: *a* from 15.84 to 16.03 Å and *c* from 7.10 to 7.25 Å.

There are many studies of the structure of tourmaline using X-ray diffraction (Hamburger and Buerger, 1948; Donnay and Buerger, 1950; Ito and Sadanaga, 1971; Buerger et al., 1962; Donnay and Barton, 1972). The b site contains the X atom in slightly distorted $XO_4(OH,F)_2$ octahedra, and the c site contains the Al atom in highly distorted $AlO_5(OH,F)$ octahedra (Buerger et al., 1962).

The color of pink tourmaline (Bradley and Bradley, 1953) is due to the absorption of light in the green-yellow and blue-violet regions of the spectrum so that the emergent light from the crystal is enriched in red and green-blue, resulting in a purple-pink tonality. This color is strongly pleochroic, intensified in the c-axis direction of the crystal. The color also changes in intensity and tonality from sample to sample. The origin of the color of pink tourmalines has been for a long time the subject of discussion among mineralogists (Manning, 1969).

Mn and Fe are present in pink tourmalines. However, the Fe concentration is generally low (Bradley and Bradley, 1953; Slivko, 1959). The color is probably due to the absorption of light by the Mn cations.

Pink tourmalines present several absorption bands between 5000 and 30 000 cm^{-1} that have been extensively studied (Manning, 1968; Wilkins et al., 1969; Manning, 1969; Bakhtin et al., 1975; Manning, 1973; Smith, 1978). There are bands whose assignments are still indefinite, mainly the 19 000-cm^{-1} band, which together with the UV-band edge is responsible for the color.

There are many types of pink tourmaline, each one reacting differently to the irradiation and annealing process (Nassau, 1975). Past studies concerning the effects of irradiation and heating on tourmalines have been performed qualitatively only for the 19 500-cm^{-1} band. We have observed that the color of the pink tourmaline can be intensified and that sometimes after irradiation, a yellow color appears mixed with the pre-existing pink. Heating at 500 °C eliminates the pink color, but the yellow color is not affected.

Our main objective is to present a comparative study by optical absorption of three kinds of pink tourmaline from Minas Gerais, Brazil, and one green sample from Goiás, Brazil. We used natural gemstones that, in the course of the experiments, were irradiated with γ-rays from a ^{60}Co source.

Experimental details

The crystals used in this study, labeled A_1 through A_4, have elongated prismatic shape with the external surfaces grooved along the crystallographic c axis. Their cross section is a rounded triangle.

The impurity concentrations of Mn and Fe are indicated in Table 1. The data show that in the pink tourmalines the Mn concentration is higher than that of Fe, whereas in green tourmalines both Mn and Fe are found in the same high proportion.

The slices used in the experiments had thicknesses of 0.65–1.65 mm. They were cut either parallel or perpendicular to the c axis (Fig. 1).

A Carl-Zeiss DMR 21 spectrophotometer was used for the optical absorption measurements. Polarized-light measurements were done with type II polaroid.

The samples were irradiated with γ-rays from a ^{60}Co source ($\sim 4 \times 10^5$ Ci) from EMBRARAD S.A. The dose was controlled by means of three processes: a ceric-cerous dosimetric system.

0003–004X/88/0102–0172$02.00

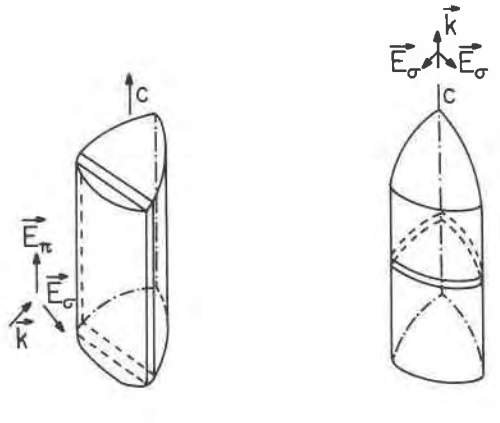

Fig. 1. Orientation of the tourmaline samples for the optical absorption measurements.

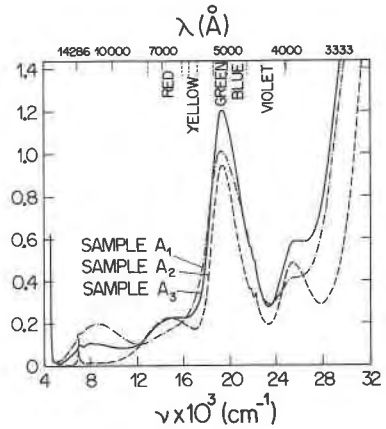

Fig. 2. Nonpolarized optical absorption spectra of three pink tourmalines. Samples cut perpendicular to the c axis.

AECL red acryllic dosimetric system, and UKAEA red perspex dosimeter.

Results of the Optical Absorption Measurements

The nonpolarized absorption spectra of tourmalines A_1, A_2, and A_3 are shown in Figure 2. For these measurements we used slices of pink tourmaline cut parallel to the (001) plane, so that $\mathbf{k} \parallel \mathbf{c}$, where $\mathbf{k}$ is the wave vector.

In Figure 3 one can see the A_4 tourmaline nonpolarized spectra. In this case, we used slices cut parallel and perpendicular to [001].

We observed absorption bands at the following approximate wave numbers:

7000 cm^{-1}. Sharp bands, typical harmonics of H_2O vibrations, present in all of the observed spectra.

8500 cm^{-1}. Wide band is observed in the pink tourmalines A_1 and A_3 and in the green tourmaline A_4. The pink tourmaline A_2 does not exhibit this band.

13 800 cm^{-1}. Wide band well characterized in A_2 and A_3 pink tourmalines and in A_4 green tourmaline. For A_1 pink tourmaline, only a shoulder is observed.

19 500 cm^{-1}. This band is the most important one in the visible region for the A_1, A_2, and A_3 pink tourmalines, but this band is absent in the spectrum for the green tourmaline.

Table 1. Concentrations of transition-metal impurities in pink and green tourmalines from X-ray fluorescence analysis

Sample	Color	Fe content (p.p.m.)	Mn content (p.p.m.)	Mn/Fe ratio
A_1	pink	390 ± 30	11 050 ± 30	28.6
A_2	pink	250 ± 20	8690 ± 30	34.8
A_3	pink	700 ± 20	11 750 ± 30	16.8
A_4	green	7450 ± 500	9000 ± 30	1.2

21 000 cm^{-1}. Observed in the pink tourmaline A_2.

23 000 cm^{-1}. Sharp and weak bands.

25 500 cm^{-1}. Observed for all three pink tourmalines, but more visible in A_2 pink tourmaline spectra, where the UV-band edge is more displaced toward UV. The A_1 and A_3 pink tourmalines show a shoulder over the UV-band edge.

Figure 4 shows the polarized optical absorption spectrum for A_2 pink tourmaline ($\mathbf{k} \perp \mathbf{c}$ cut). In this case, the spectra vary significantly with the polarization angle for the 19 500-cm^{-1} and 25 500-cm^{-1} bands. The 19 500-cm^{-1} band moved in the UV direction and decreased with the polarization angle. We attributed this behavior to the strong reduction of the absorption of the 19 500-cm^{-1} band; the reduction allowed another absorption band around 21 000 cm^{-1} to show.

Figure 5 shows the change in absorption intensities for the $\mathbf{k} \perp \mathbf{c}$ cut of pink tourmaline A_2, plotted as a function of the polarization angle for the bands at 13 800, 19 500,

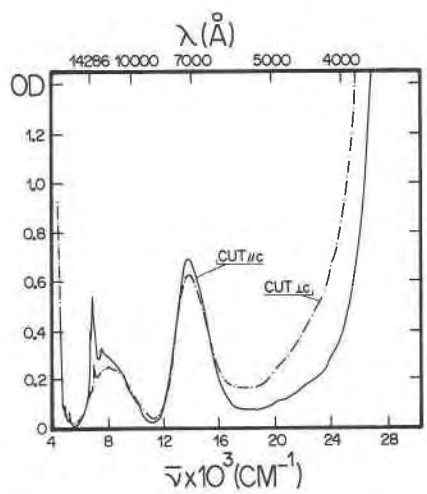

Fig. 3. Nonpolarized optical absorption spectra of the green tourmaline. Sample A_4 cut parallel and perpendicular to the crystallographic axis.

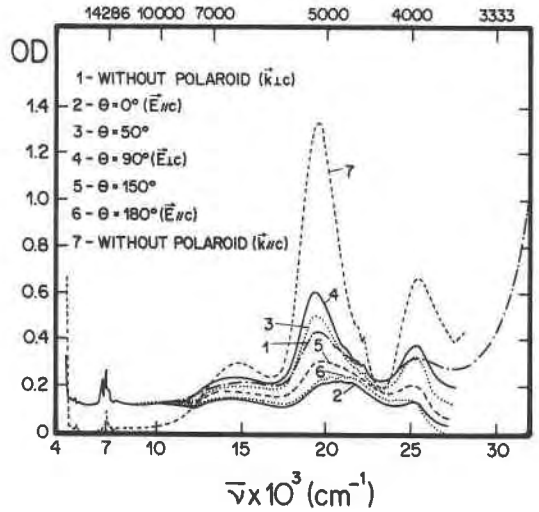

Fig. 4. Polarized measurements. Sample A_2 cut parallel to the c axis.

and 25 500 cm^{-1}. The 19 500- and 25 500-cm^{-1} bands behave similarly; their absorption intensities change strongly with the polarization angle. The 13 800-cm^{-1} band, however, is hardly affected by the polarization angle.

The A_1, A_3, and A_4 tourmaline spectra show a band at 8500 cm^{-1}, but we cannot see such a band in the A_2 spectra. On the other hand, the 13 800-cm^{-1} band has an intermediate intensity in the A_2, A_3, and A_4 tourmaline

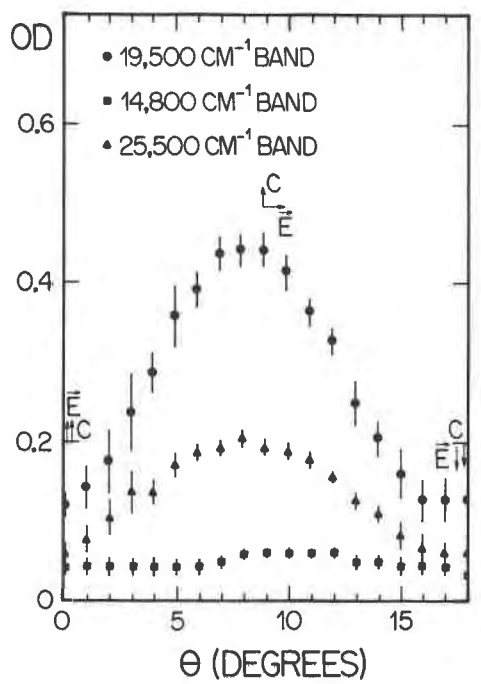

Fig. 5. Intensity of the absorption bands as a function of the polarization angle of the electric field direction. Sample A_2 cut parallel to c axis.

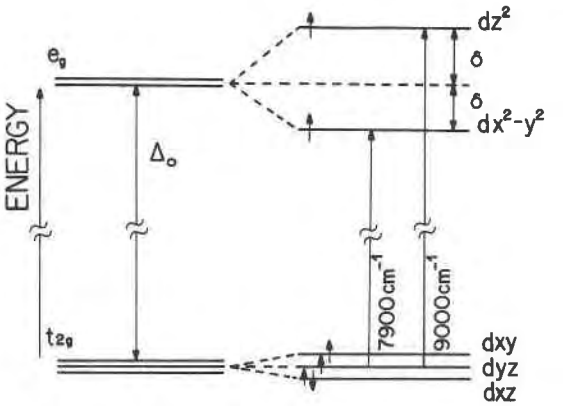

Fig. 6. Energy-level diagram of the Fe^{2+} in the b site.

spectra, but is weak in the A_1 spectrum. From all these observations, we can conclude that those two bands are not connected to each other. Thus, the doublet hypothesis proposed by Smith (1978) in those two band assignments can be eliminated. Moreover, as those two bands are observed in the A_3 and A_4 spectra, where the Fe content is larger than in the other samples, it reinforces the more accepted suggestion that those bands are Fe absorption bands. On this basis and in accordance with Faye et al. (1968), Burns (1972), and Burns and Simon (1973), we tentatively assigned the 8500-cm^{-1} band to Fe^{2+} absorption in the b site. Because the b site is only slightly distorted, the Fe^{2+} ($3d^6$) has a high-spin configuration ($s = 2$), being situated in a weak oxygen field. The energy-level diagram is shown in Figure 6. The δ and Δ_o parameters according to the scheme in Figure 6 are $\delta = 550$ cm^{-1} and $\Delta_o = 8450$ cm^{-1}.

An absorption band is observed at 13 800 cm^{-1} for the A_4 green tourmaline, and it is displaced to 14 800 cm^{-1} in the pink tourmalines. This is because of the strong band edge from the 19 500-cm^{-1} band, which is the most intense band of the pink tourmalines. According to Smith (1978), the 13 800-cm^{-1} band is a doublet located at 13 400 and 13 800 cm^{-1}.

The 13 800-cm^{-1} band value is between the lower-energy 12 000-cm^{-1} Fe^{2+} electronic transition observed in beryl (Blak et al., 1982) and the higher-energy 16 000-cm^{-1} Mn^{4+} spin-forbidden transition observed in K_2MnF_6 (Jørgensen, 1958) and interpreted to also exist in spodumene (Cohen and Janezic, 1983). The Fe^{2+} in highly distorted c site, with a higher crystal-field strength, can account for this band. The splitting shown by Smith (1978) could be assigned to the unfolding of the d_{xz} and d_{yz} levels, which is due to the orthorhombic component of the crystal field. This assumption is reinforced by the fact that the band present in spectra from A_2 tourmaline, which has an Fe content of 250 ppm, makes less probable the assumption of the Fe-Fe charge-transfer interaction. However, distortion might be a cause of pleochroism. As no pleochroism was observed, it makes less probable the assignment of the 13 800-cm^{-1} band to Fe^{2+} absorption in the c site.

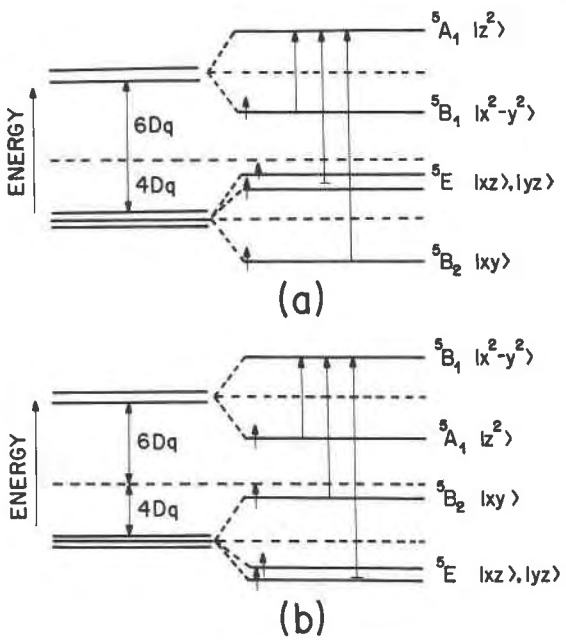

Fig. 7. (a) Energy-level diagram of the Mn^{3+} in a compressed octahedron along the z axis. (b) Energy-level diagram of the Mn^{3+} in an elongated octahedron along the z axis.

A less distorted b site with lower crystal-field strength could account for the lowering of the Mn^{4+} spin-forbidden 16 000-cm^{-1} transition to 13 800 cm^{-1}. However, we must point out that the Mn concentration in the present tourmaline is about 20 times lower than in K_2MnF_6 and that lower distortion decreases the mixing of the electronic orbitals, which account for the lifting of the forbidden-transition probability. Boith considerations suggest that the absorbance of Mn^{4+} in tourmaline is much less than in K_2MnF_6. Thus this assignment is also less probable.

We conclude that the present data for the 13 800-cm^{-1} band do not allow a conclusive assignment.

The 21 000-cm^{-1} band, present in the A_2 tourmaline spectrum in the optical absorption measurement using polarized light, could be the 21 600-cm^{-1} band observed in green tourmalines. Because of the low absorption observed, the low Fe concentration, and the high absorption expected for an Fe-Fe interaction band, we adopt the same assignment as Smith (1978).

The sharp bands at 23 000 cm^{-1} are due to the transitions $^6A_1 \rightarrow {}^4A, {}^4E$ belonging to Mn^{2+} (MacClure, 1959) or to Mn^{3+} (Marfunin, 1979, p. 214), but precise assignment is not possible because of the low intensity of these bands.

When we have tourmalines with a high Fe content, the UV-band edge is displaced to low values. This type of UV cutoff has been very satisfactorily explained by O^{2-}–Fe^{3+} charge transfer (Loeffler and Burns, 1976).

The 19 500-cm^{-1} band is common to all the pink tourmalines studied. The polarization spectra suggest that this band is related to the 25 500-cm^{-1} band. This result reinforces the assignments of Bakhtin et al. (1975) and Manning (1968, 1969, 1973), that is, that the band is due to the Mn^{3+} ion. By analogy with epidote (Burns and Strens, 1967) and spodumene (Ito, 1980), we suggest that these bands are due to Mn^{3+} in the b site.

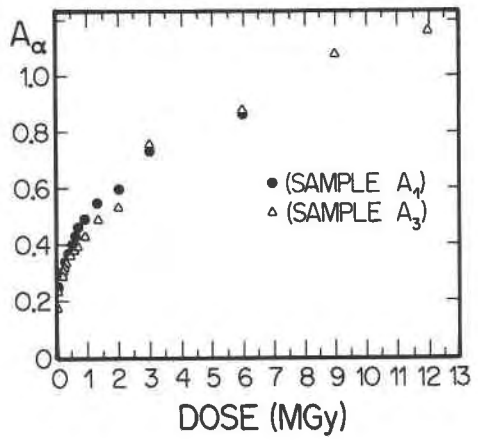

Fig. 8. Growth of the 19 500-cm^{-1} band with the irradiation dose. Samples A_1 and A_3 cut perpendicular to the c axis.

Optical absorption spectroscopy analyzed according to crystal field theory

The Mn^{3+} ion is stabilized in the b site by a Jahn-Teller distortion along the O(1)H-O(3)H axis. The electrical potential is

$$V_c + V_{D4},$$

where V_c is the cubic distortion potential and V_{D4} is the tetragonal distortion potential. The matrix elements are

$$\begin{aligned}
\langle d_{x^2-y^2}|V_c|d_{x^2-y^2}\rangle &= \langle d_{z^2}|V_c|d_{z^2}\rangle = 6Dq;\\
\langle d_{xy}|V_c|d_{xy}\rangle &= \langle d_{xz}|V_c|d_{xz}\rangle = \langle d_{yz}|V_c|d_{yz}\rangle = 4Dq;\\
\langle d_{x^2-y^2}|V_{D4}|d_{x^2-y^2}\rangle &= 2Ds - Dt;\\
\langle d_{z^2}|V_{D4}|d_{z^2}\rangle &= -2Ds - 6Dt;\\
\langle d_{xy}|V_{D4}|d_{xy}\rangle &= 2Ds - Dt;\\
\langle d_{xz}|V_{D4}|d_{xz}\rangle &= \langle d_{yz}|V_{D4}|d_{yz}\rangle = -Ds + 4Dt.
\end{aligned}$$

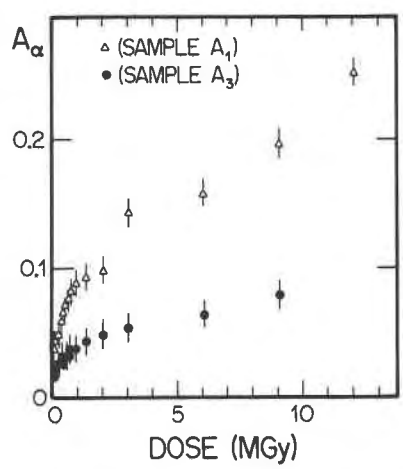

Fig. 9. Growth of the 8500-cm^{-1} band with the irradiation dose. Samples A_1 and A_3 cut perpendicular to the c axis.

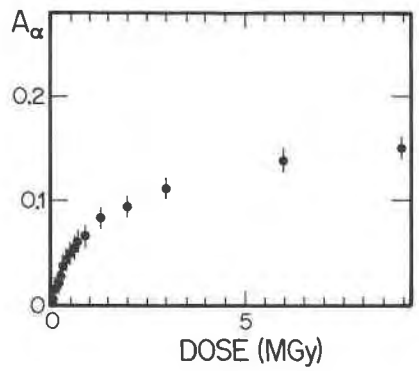

Fig. 10. Growth of the 25 500-cm^{-1} band with the irradiation dose. Sample A_3 cut perpendicular to the c axis.

We must consider two cases:

1. Octahedral site compressed along the *z* axis. The energy-level diagram is shown in Figure 7a. The transition energies are

$$E(^5A_1) - E(^5B_1) = -4Ds - 5Dt$$
$$E(^5A_1) - E(^5E) = 10Dq - Ds - 10Dt = 19\,500\ cm^{-1}$$
$$E(^5A_1) - E(^5B_2) = 10Dq - 4Ds - 5Dt = 25\,500\ cm^{-1}.$$

Using the value $Dq = 1100\ cm^{-1}$ employed by Ito (1980), in order to explain the Mn^{3+} center in spodumene, we obtain:

$$Dt = -557\ cm^{-1}$$
$$Ds = -2920\ cm^{-1}.$$

The quotient Ds/Dt is 5.3, and the Ds and Dt values

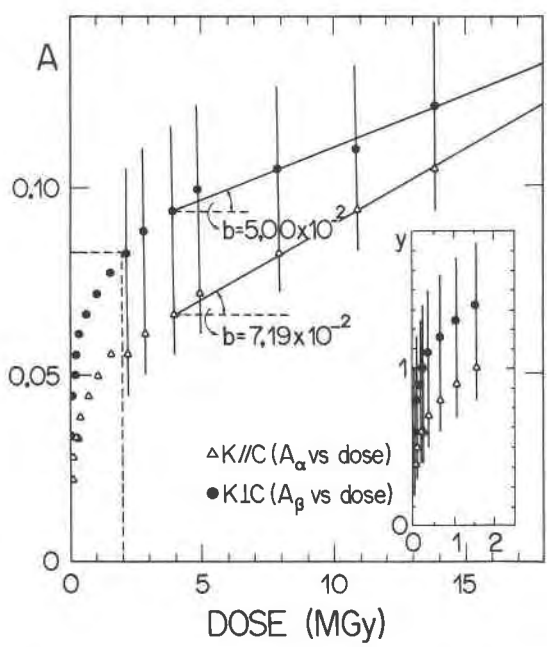

Fig. 11. Growth of the 14 800-cm^{-1} band with the irradiation dose. Sample A_2 cut parallel and perpendicular to the c axis.

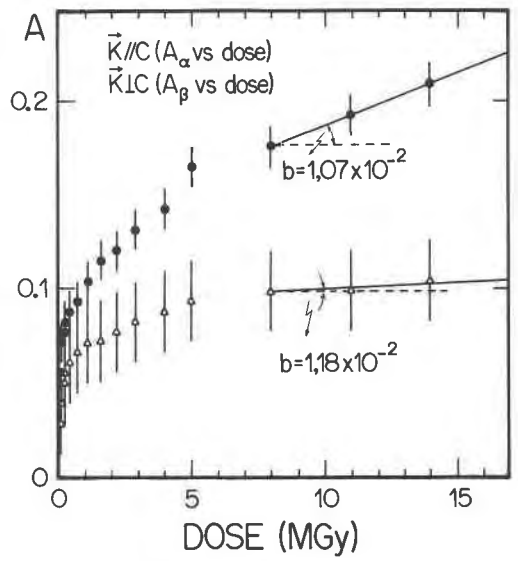

Fig. 12. Growth of the 25 500-cm^{-1} band with the irradiation dose. Sample A_2 cut parallel and perpendicular to the c axis.

are comparable to those obtained in spodumene. We obtain

$$E(^5A_1) - E(^5B_1) = 14\,500\ cm^{-1}.$$

This transition was not observed, probably because it was too weak and was hidden by the absorption at 13 800 cm^{-1}.

The crystal-field stabilization energy (CFSE) is given by

$$CFSE = \tfrac{3}{5}(10Dq) + \tfrac{1}{2}|E(^5A_1) - E(^5B_1)|.$$

Using the above values, we obtain

$$CFSE = 37.9\ kcal/mol.$$

2. Octahedral site elongated along the *z* axis. The energy-level diagram is shown in Figure 7b. The transition energies are

$$E(^5B_1) - E(^5A_1) = 4Ds + 5Dt$$
$$E(^5B_1) - E(^5B_2) = 10Dq = 19\,500\ cm^{-1}$$
$$E(^5B_1) - E(^5E) = 10Dq + 3Ds - 5Dt = 25\,500\ cm^{-1}.$$

Using the $Ds = 5Dt$ approximation, we obtain

$$Dq = 1950\ cm^{-1}$$
$$Ds = 3000\ cm^{-1}$$
$$Dt = 600\ cm^{-1}$$

and

$$CFSE = 54.9\ kcal/mol.$$

The Dq and CFSE results, compared with results obtained for other crystals (Dunitz and Orgel, 1957; MacClure, 1957), are compatible with the octahedral site compressed along the O(1)H-O(3)H axis.

Therefore, we assign the 19 500-cm^{-1} band to the Mn^{3+} absorption in the b site compressed along the O(1)H-O(3)H axis.

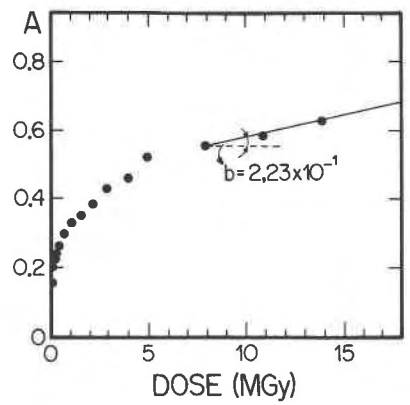

Fig. 13. Growth of the 19 500-cm^{-1} band with the irradiation dose. Sample A_2 cut perpendicular to the c axis.

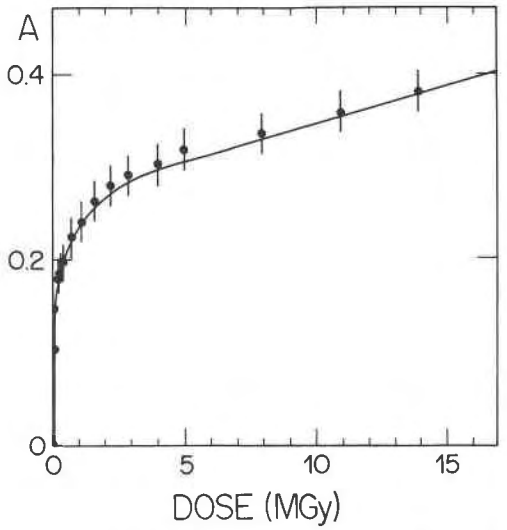

Fig. 14. Growth of the 19 500-cm^{-1} band with the irradiation. Fit according to Levy's model. Sample A_2 cut parallel to the c axis.

Irradiation results

The pink tourmalines A_1, A_2, and A_3 had their color accentuated by irradiation processes. The green tourmaline A_4 became pink.

We observed that the coloring process in tourmaline is reversible. Heating to 600 °C for some hours changes tourmaline from pink to colorless. The lost color can be restored by the irradiation process.

A_1 and A_3 pink tourmalines

The dose curve of the 19 500-cm^{-1} band referring to the A_1 and A_3 pink tourmaline spectra, where **k** ∥ **c**, can be seen in Figure 8. Both show a quick initial growth of the 19 500-cm^{-1} band, with a tendency to saturate in 2.00 MGy (100 rads = 1 Gy). Following this, there is another sharp rise. This new growth seems to be composed of a new saturation curve, which we believe to be a supersaturation curve with a linear growth for doses higher than those used by us in this work.

In Figure 9, we present the dose curve of the 8500-cm^{-1} band again for the A_1 and A_3 pink tourmalines, where **k** ∥ **c**. We notice behavior similar to that observed to the 19 500-cm^{-1} band with a step in 2.00 MGy.

In Figure 10, a dose curve for the 25 500-cm^{-1} band is shown only for A_3 spectra, where **k** ∥ **c**. For this band, a small step is observed at 2.00 MGy.

When we bleach the A_1 and A_3 pink tourmalines, their spectra reveal a band at 32 000 cm^{-1} (A_1) and a shoulder at 30 000 cm^{-1} (A_3).

A_2 pink tourmaline

The A_2 pink tourmaline has a low-Fe concentration and a low UV-band edge. The dose curves for the 13 800-cm^{-1} band, where **k** ⊥ **c** and **k** ∥ **c**, are shown in Figure 11. We observe that a linear growth begins at 4.00 MGy. For **k** ∥ **c**, we note a step around 2.00 MGy, followed by supersaturation.

The dose curves for the 25 000-cm^{-1} band, where **k** ∥ **c** and **k** ⊥ **c**, are shown in Figure 12. We observe that from 8.00 MGy, a linear growth begins. Here, for **k** ∥ **c**, we also notice a step at 2.00 MGy, followed by supersaturation.

The dose curve for the 19 500-cm^{-1} band, where **k** ∥ **c**, is shown in Figure 13. We observe a step at 2.00 MGy, followed by supersaturation and linear growth from 8.00 MGy. In Figure 14, for **k** ⊥ **c**, we do not observe the step, and growth is linear from 4.00 MGy.

In Figure 15 we show the correlation among the absorbances of the bands at 19 500 vs. 25 500 cm^{-1} for the A_2 pink tourmaline obtained from the dose curves. These curves produce correlations that are approximately linear. The curves for **k** ∥ **c** and **k** ⊥ **c** are coincident, showing the same polarization effects.

In Figure 16, we show the correlation between the absorbances of the 19 500-cm^{-1} band measured for **k** ∥ **c** (A_α) and **k** ⊥ **c** (A_β). We notice a deviation from the linear behavior in $D = 2.20$ MGy. This deviation of the behavior is seen in the small step in Figure 13. This supersaturation phenomenon makes it difficult to analyze the dose curve growth.

The dose curve, where **k** ⊥ **c**, of the 19 500-cm^{-1} band is quite regular. Thus, we have made an empirical adjustment of this dose curve. We believe that the best model to do this adjustment is Levy's model (Levy et al., 1974):

$$y = \sum_{i=1}^{3} \alpha_i |1 - e^{-\beta_i D}| + \gamma D,$$

where γ is the angular coefficient of the linear part of the experimental curve, D is the irradiation dose to which the sample was submitted, β_i is a constant that expresses the ith center growth rate, and the α_i values are the contributions of each center.

The fitting curve is

$$y = 0.954(1 - e^{-55.800}) + 1.970(1 - e^{-13.00D}) + 1.926(1 - e^{1.01D}) + 0.143D,$$

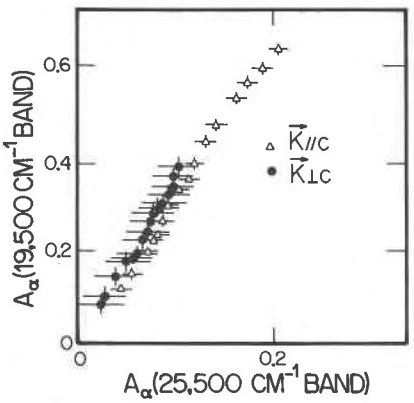

Fig. 15. Correlation between the growth of the 19 500- and 25 500-cm^{-1} bands as a function of the irradiation dose for sample A_2.

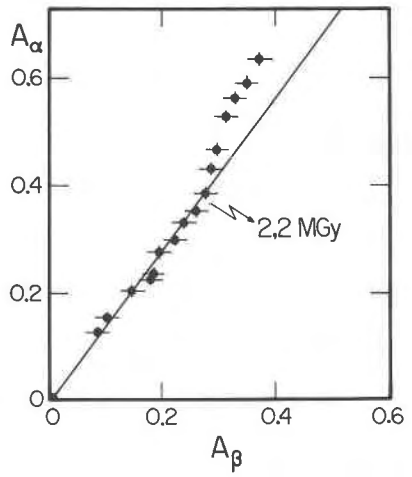

Fig. 16. Correlation between the growth of A_α and A_β as a function of the irradiation dose for the 19 500-cm^{-1} band for sample A_2.

where the dose is measured in megagrays (MGy). The adjusted curve is the full line in Figure 14. This fit shows that the radiation-growth kinetics are very complex and must be analyzed with regard to a microscopic model.

Discussion

We assigned to the b and c sites the position of the ions responsible for the absorptions observed in this study. Let us examine the occupation possibilities of octahedrally coordinated metals in these sites. The b site is formed by the $XO_4(OH,F)_2$ octahedron. There are three sites, b_1, b_2, and b_3, that have a common (OH,F) group in the O(1)H site. The structural analysis is very complex because the X site can be occupied by ions having a charge of 1+, 2+, 3+, and 4+ and because the vertex of the three b sites can be occupied by either OH^- or F^-. Let us consider, in this discussion, the b sites of the $XO_4(OH)_2$ type. The X ions are octahedrally coordinated by four oxygens in the plane perpendicular to the octahedral axis, with an OH^- group on each vertex. In dravite, where X = Mg^{2+}, the octahedra are oriented along the O(1)H-O(3)H axis (Buerger et al., 1962), and the hydroxyl O(1)H connects the sites b_1, b_2, and b_3. In elbaite, where X = Al^{3+} or Li^+, the alignment of the octahedra along the O(1)H-O(3)H axis can be distorted.

The c sites are formed by $YO_5(OH)$ octahedra, and they are occupied mainly by Al^{3+}.

The O(3)H group is shared by a b site and a c site. There are six c sites in the brucite structure, which may be considered as part of the dravite structure.

The average Mg–O distance in dravite for the b site is $\simeq$2.06 Å and for the c site is $\simeq$1.93 Å (Donnay and Buerger, 1950). In M^{2+} oxides having structures similar to NaCl, the Mn–O distance (Hush, 1958) is 2.25 Å. As Mn^{2+} has a d^5 configuration, it is not susceptible to Jahn-Teller distortions in sixfold coordination sites. Thus the Mn^{2+} is too large to occupy the b and c sites.

In $LaM^{3+}O_3$, which has a perovskite structure (Hush and Pryce, 1957, 1958), the Mn–O distance is ~1.97 Å, showing that the Mn^{3+} possibly can be accommodated in the b and c sites, preferably in the b sites. Furthermore, Mn^{4+}, having a smaller ionic radius than Mn^{3+}, possibly can be accommodated in the b and c sites.

The Fe–O distance in $LaM^{3+}O_3$ is ~1.97Å, so that the Fe^{3+} possibly can be accommodated in the b and c sites, preferably in the b site. On the other hand, Fe–O distances in oxides having the same structure as NaCl are ~2.16 Å and are therefore greater than the M–O distance for the b and c sites. However, Fe^{2+} is a d^6-configuration ion, susceptible to Jahn-Teller distortions in sixfold coordination sites. The b and c sites are distorted so that they can accommodate the Fe^{2+}.

We conclude that the b and c sites can accommodate Mn^{3+}, Fe^{2+}, and Fe^{3+}, with a higher probability for these ions being in the b site.

Let us now analyze the results obtained from the polarization measurements and the dose curves. The intensities of the 19 500-cm^{-1} band do not depend on the direction of **E** for samples with **k** $\parallel$ **c**. The polarization of those bands with **k** $\perp$ **c** reaches a maximum with **E** $\perp$ **c** and a minimum with **E** $\parallel$ **c**. As the polarization of the bands at 19 500 and 25 500 cm^{-1} shows the same features, we have assigned them to the same coloring agent. The plots of A_α for 19 500 cm^{-1} vs. A_α for 25 500 cm^{-1} compared for samples with **k** $\parallel$ **c** and those with **k** $\perp$ **c** (Fig. 15) lie on the same straight line, reinforcing the assignment of these bands to only one center.

The dichroism phenomenon in the pink tourmaline, resulting from the polarization of the absorption bands, has been discussed by several authors. Attempts have been made to explain it by means of two models:

1. Wilkins's model (Wilkins et al., 1969). The (111) axis of the b site is parallel to the **c** axis, but does not coincide with the C_3 axis. This axis is situated in the

brucite structure center, crossing the O(1)H site, and is parallel to the **c** axis. The intensity of the absorption could be due to the expansion of the crystal field in odd terms. In this case the Hamiltonian is

$$H_{cubic} + H_{odd\text{-}trigonal} + H_{even\text{-}tetragonal}.$$

This Hamiltonian transforms itself neither according to the operations from the C_3 group nor the C_∞ group. Besides, it does not have the inversion symmetry in the trigonal plan. Thus, this model does not explain the polarization of the bands at 19 500 and 25 500 cm^{-1}.

2. Townsend's model (Townsend, 1970). As there is no unique distortion along the **c** axis, the dependence of absorption intensity on polarization should be due to either the interactions with the neighboring sites or the composed spectrum symmetry.

This last model would contribute to the dichroism of tourmaline if the transitions within the individual b sites were polarized along the O(1)H-O(3)H axis. The resultant spectrum would be polarized with regard to the **c** axis, and the absorption coefficient ratio, α, for $\mathbf{E} \parallel \mathbf{c}$ and for $\mathbf{E} \perp \mathbf{c}$ is between 1 and 1.73. Nevertheless, in this model, we should expect threefold symmetry in the intensity of the spectrum polarized with **E** on the plane perpendicular to the **c** axis. Besides, we should expect that the maximum values on the plane parallel to the **c** axis should occur at 63° from the **c** axis. Those behaviors differ from the results reported in this paper.

We observe that the band at 19 500 cm^{-1} for sample A_2 with $\mathbf{k} \parallel \mathbf{c}$ and $\mathbf{E} \perp \mathbf{c}$ has absorbance $A_\alpha \simeq 0.78$, and with $\mathbf{k} \perp \mathbf{c}$ and $\mathbf{E} \perp \mathbf{c}$, $A_\beta \simeq 0.45$. This means that different absorbance values, A_α and A_β, were observed for the same direction of the electric field radiation. For $\mathbf{k} \parallel \mathbf{c}$, the magnetic field radiation, **H**, is perpendicular to the **c** axis; and for $\mathbf{k} \perp \mathbf{c}$ and $\mathbf{E} \perp \mathbf{c}$, **H** is parallel to the **c** axis, i.e., **H** of A_α is perpendicular to **H** for A_β. Thus, the difference between A_α and A_β shows a magnetic dipole transition contribution. Although a magnetic dipole process is weaker than an electric dipole process—since the maximum possible values of the matrix elements $\langle f|\boldsymbol{\mu}\cdot\mathbf{B}|i\rangle$ (where i, f = initial and final states, $\boldsymbol{\mu}$ = magnetic dipole operator, **B** = the strength of the magnetic field radiation) are weaker than the possible values of the matrix elements of $\langle f|\mathbf{p}\cdot\mathbf{E}|i\rangle$ (where **p** = electric dipole moment operator)—a magnetic dipole process may occur when a radiative transition is forbidden by an electric dipole process (Imbusch, 1978, p. 23). This possibility is consistent with the assignment of the 19 500-cm^{-1} band to the ${}^5E \rightarrow {}^5A$ electric dipole spin-forbidden transition (in octahedral symmetry, *d* orbitals are symmetric and so $\langle f|\mathbf{p}\cdot\mathbf{E}|i\rangle = 0$) allowed by distortion of the octahedra.

The heating of the pink tourmaline to 600 °C for some hours produces the complete decay of the bands responsible for the color (19 500 cm^{-1} and the UV-band edge), making it become almost colorless. By irradiation with γ-rays from ^{60}Co, the color is recomposed by the increase in the absorption bands. These bands increase quickly up to 1.00 MGy, when they start to become saturated.

TABLE 2. Possible combinations for Mn substitution

Combination	X_1	X_2	X_3	Charge
I	Li^+	Al^{3+}	Mn^{2+}	6+
II	Li^+	Li^+	Mn^{4+}	6+

Figure 16 shows two phases in the growth relation of A_α vs. A_β for the 19 500-cm^{-1} band in sample A_2. In the first phase up to 2.00 MGy, A_α and A_β increase at the same rate, keeping the ratio A_α/A_β constant (about 1.4). With additional radiation, a second phase of growth occurs in which A_α increases at a rate higher than A_β, giving $A_\alpha/A_\beta > 1.4$. These observations suggest the existence of at least two color centers, I and II. Center I predominates in the first growth phase of the absorption band, and center II starts to appear in significant concentrations in the second phase.

The increase of the A_α/A_β ratio in the second phase is mainly due to more accentuated growth of A_α, rather than to decreased growth of A_β. We suggest that this increase occurs because center II absorbs more with $\mathbf{k} \parallel \mathbf{c}$ polarization (A_α) and less with $\mathbf{k} \perp \mathbf{c}$ polarization (A_β). As the contribution to the transition for $\mathbf{E} \perp \mathbf{c}$ is the same in A_α and A_β, we suggest that the dichroism of the magnetic dipole transition is higher in center II.

The dose curves of the 19 500- and 25 500-cm^{-1} bands for samples A_1 and A_3 show phases of saturation, supersaturation, and linear growth. We attribute the saturation phase to the predominance of center I and the supersaturation to the presence of center II.

The skeleton of the brucite structure has the formula $[XO_4(OH,F)]_3(OH,F)$ with X having a charge of +2e. Thus, the total charge at the b sites in brucite will be +6e. Without changing the total charge of brucite, we have two principal combinations for Mn substitution (Table 2).

Combination I has low probability, because Mn^{2+} is too large to occupy the b site. EPR measurements do not show the sharp lines characteristic of Mn^{2+}, reinforcing the present suggestion that Mn is not found as Mn^{2+} in the tourmalines studied here. Combination II has a high probability because Mn^{4+} is small enough to occupy the b site.

The charge of X in $XO_4(OH,F)$ is 2+, which means that Mn^{4+} will produce a high localized 2+ charge, turning the b site into an electron trap. On the other hand, the b site with Li^+ will produce a localized charge of 1− turning this site into a hole trap.

Irradiation will produce conduction electrons and valence holes, which can be trapped by Mn^{4+} in the b site (i.e., an electron trap) and by Li^+ in the b site (i.e., a hole trap). Because of the difference between the site expectation (2+) and the effective charge of Mn^{4+} (4+), it is possible that Mn^{4+} undergoes transitions to Mn^{3+} when Mn^{4+} in the b site captures one conduction electron. Thus, we assign the precursor center for the 19 500-cm^{-1} band to Mn^{4+} in the b site.

Acknowledgments

We are grateful to Mr. Beppe, J.R.M. Fortunato, and M. Blum for the samples, to Prof. O. L. Dias (UFGo) for the X-ray fluorescence measurements, to EMBRARAD S.A. for the use of their ^{60}Co γ-rays source, and to Prof. Dr. Walter M. Pontuschka for the discussions that enriched this work. This work was supported by grants from CAPES, CNPq, FAPESP, and FINEP.

References cited

Bakhtin, A.I., Minko, O.Ye., and Vikonurov, V.M. (1975) Isomorphism and colour of tourmaline. Izvestiya Akademii Nauk SSRR, Seriya Geologicheskaya, 6, 73–83.

Barton, R., Jr. (1969) Refinement of crystal structure of buergerite and the absolute orientation of tourmalines. Acta Crystallographica, B25, 1524–1533.

Blak, A.R., Isotani, S., and Watanabe, S. (1982) Optical absorption and electron spin resonance in blue and green natural beryl. Physics and Chemistry of Minerals, 8, 161–166.

Bradley, J.E.S., and Bradley, O. (1953) Observations on the colouring of pink and green zoned tourmaline. Mineralogical Magazine, 30, 26–38.

Buerger, M.J., Burnham, C.W., and Peacor, D.R. (1962) Assessment of several structures proposed for tourmaline. Acta Crystallographica, 15, 583–590.

Burns, R.G. (1972) Mixed valencies and site occupancies of iron in silicate minerals from Mössbauer spectroscopy. Canadian Journal of Spectroscopy, 17, 51–59.

Burns, R.G., and Simon, H.F. (1973) Cation disorder in tourmalines. Geological Society of America Abstracts with Programs, 5, 563–564.

Burns, R.G., and Strens, R.G.J. (1967) Structural interpretation of polarized absorption spectra of Al-Fe-Mn-Cr-epidotes. Mineralogical Magazine, 35, 547.

Cohen, A.J., and Janezic, G.G. (1983) The crystal-field spectra of the $3d^3$ ions, Cr^{3+} and Mn^{4+}, in green spodumenes, the significance of trace elements in solving petrogenetic problems & controversies. Theophrastus Publications S.A., Athens, 899–904.

Donnay, G., and Barton, R. (1972) Refinement of the crystal structure of elbaite and the mechanism of tourmaline solid solution. Tschermaks Mineralogische und Petrographische Mitteilungen, 18, 273–286.

Donnay, G., and Buerger, M.J. (1950) The determination of the crystal structure of tourmaline. Acta Crystallographica, 3, 379–388.

Dunitz, J.D., and Orgel, L.E. (1957) Electronic properties of transition element oxides. II. Cation distribution amongst octahedral and tetrahedral sites. Journal of Physics and Chemistry of Solids, 3, 318–330.

Faye, G.H., Manning, P.G., and Nickel, E.H. (1968) An interpretation of the polarized optical absorption spectra of tourmaline, cordierite, chloritoid and vivianite: Fe^{2+}-Fe^{3+} electronic interaction as a source of pleochroism. American Mineralogist, 53, 1174–1201.

Hamburger, G.E., and Buerger, M.J. (1948) The structure of tourmaline. American Mineralogist, 33, 532–540.

Hush, N.S. (1958) Crystal field stabilization and site deformation in crystals and complexes containing ions. Discussion of the Faraday Society, 26, 145.

Hush, N.S., and Pryce, M.H.L. (1957) Radii of transition ions in crystals fields. Journal of Chemical Physics, 26, 143–144.

——— (1958) Influence of the crystal field potential on interionic separation in salts of divalent iron-group ions. Journal of Chemical Physics, 28, 424–429.

Imbusch, G.F. (1978) Inorganic luminescence. In M.D. Lumb, Ed., Luminescence spectroscopy. Academic Press, New York.

Ito, A.S. (1980) Study of radiation damage and heat treatment in spodumene. Ph.D. thesis, University of São Paulo, São Paulo, Brazil.

Ito, A.S., and Sadanaga, R.L. (1971) A Fourier analysis of the structure of tourmaline. Acta Crystallographica, 4, 385–390.

Jørgensen, C.K. (1958) Acta Chemica Scandinava, 12, 1539 (not seen; extracted from Cohen and Janezic, 1983).

Levy, P.W., Mattern, P.L., Lengweiler, K., and Bishay, A. (1974) Studies on nonmetals during irradiation: V. Growth and decay of color centers in barium aluminoborato glasses containing cerium. American Ceramic Society Journal, 57, 176–181.

Loeffler, B.M., and Burns, R.G. (1976) Shedding light on the color of gems and minerals. American Scientist, 64, 636–647.

MacClure, D.S. (1957) The distribution of transition metal cations in spinels. Journal of Physics and Chemistry of Solids, 3, 311–317.

——— (1959) Electronic spectra of molecules and ions in crystals: Part II. Spectra of ions in crystals. Solid State Physics, 9, 399–525.

Manning, P. G. (1968) Absorption spectra of the manganese-bearing chain silicates, pyroxmangite, rhodonite, bustanite and serandite. Canadian Mineralogist, 9, 348–357.

——— (1969) An optical absorption study of the origin of colour and pleochroism in pink and brown tourmalines. Canadian Mineralogist, 9, 678–690.

——— (1973) Effect of second-nearest-neighbour interaction on Mn^{3+} absorption in pink and black tourmalines. Canadian Mineralogist, 11, 971–977.

Marfunin, A.S. (1979) Physics of minerals and inorganic materials. Springer-Verlag, New York.

Nassau, K. (1975) Gamma-ray irradiation–induced changes in the color of tourmaline. American Mineralogist, 60, 710–713.

Slivko, M.S. (1959) Manganese tourmalines. Mineralogiskii Sbornik (L'vov), 13, 139 (translated in International Geological Review, 195, 1961).

Smith, G. (1978) A reassessment of the role of iron in the 5000–30,000 cm^{-1} region of the electronic spectra of tourmaline. Physics and Chemistry of Minerals, 3, 343–373.

Townsend, M.G. (1970) On the dichroism of tourmaline. Journal of Physics and Chemistry of Solids, 1, 2481–2488.

Webster, R. (1980) Gems, their sources, description and identification. Butterworths, London, Boston.

Wilkins, R.W.T., Farrell, E.F., and Naiman, C.S. (1969) The crystal field spectra and dichroism or tourmaline. Journal of Physics and Chemistry of Solids, 30, 43–56.

Manuscript received July 28, 1986
Manuscript accepted September 14, 1987